





Spike Protein Cleavage-Activation in the Context of the SARS-CoV-2 P681R Mutation: an Analysis from Its First Appearance in Lineage A.23.1 Identified in Uganda

Bailey Lubinski,^{a,b} Laura E. Frazier,^a My V. T. Phan,^c Daniel L. Bugembe,^c Jessie L. Cunningham,^a Tiffany Tang,^d Susan Daniel,^d Matthew Cotten,^{c,e}  Javier A. Jaimes,^b  Gary R. Whittaker^{b,f}

^aGraduate Program in Biological & Biomedical Sciences, Cornell University, Ithaca, New York, USA

^bDepartment of Microbiology and Immunology, College of Veterinary Medicine, Cornell University, Ithaca, New York, USA

^cMRC/UVRI and London School of Hygiene and Tropical Medicine – Uganda Research Unit, Entebbe, Uganda

^dRobert Frederick Smith School of Chemical and Biomolecular Engineering, Cornell University, Ithaca, New York, USA

^eMRC Centre of Virus Research, University of Glasgow, Glasgow, United Kingdom

^fDepartment of Public and Ecosystem Health, College of Veterinary Medicine, Cornell University, Ithaca, New York, USA

Bailey Lubinski and Laura E. Frazier contributed equally to this article. Author order was determined on the basis of contribution.

ABSTRACT Based on its predicted ability to affect transmissibility and pathogenesis, surveillance studies have highlighted the role of a specific mutation (P681R) in the S1/S2 furin cleavage site of the SARS-CoV-2 spike protein. Here we analyzed A.23.1, first identified in Uganda, as a P681R-containing virus several months prior to the emergence of B.1.617.2 (Delta variant). We performed assays using peptides mimicking the S1/S2 from A.23.1 and B.1.617 and observed significantly increased cleavability with furin compared to both an original B lineage (Wuhan-Hu1) and B.1.1.7 (Alpha variant). We also performed cell–cell fusion and functional infectivity assays using pseudotyped particles and observed an increase in activity for A.23.1 compared to an original B lineage spike. However, these changes in activity were not reproduced in the B lineage spike bearing only the P681R substitution. Our findings suggest that while A.23.1 has increased furin-mediated cleavage linked to the P681R substitution, this substitution needs to occur on the background of other spike protein changes to enable its functional consequences.

IMPORTANCE During the course of the SARS-CoV-2 pandemic, viral variants have emerged that often contain notable mutations in the spike gene. Mutations that encode changes in the spike S1/S2 (furin) activation site have been considered especially impactful. The S1/S2 change from proline to arginine at position 681 (P681R) first emerged in the A.23.1 variant in Uganda, and subsequently occurred in the more widely transmitted Delta variant. We show that the A.23.1 spike is more readily activated by the host cell protease furin, but that this is not reproduced in an original SARS-CoV-2 spike containing the P681R mutation. Changes to the S1/S2 (furin) activation site play a role in SARS-CoV-2 infection and spread, but successful viruses combine these mutations with other less well identified changes, occurring as part of natural selection.

KEYWORDS A.23.1, P681R mutation, SARS-CoV-2, spike, Uganda

Severe acute respiratory syndrome coronavirus 2 (SARS-CoV-2) is the agent causing the current COVID-19 pandemic (1). SARS-CoV-2 was first identified in late 2019 and has since spread rapidly throughout the world. The virus emerged as two main lineages, A and B, and now multiple sublineages. While the B.1 lineage became the dominant virus following its introduction into Northern Italy and spread through Europe/UK in February 2020, both A and B lineages remain in circulation globally (2). Both lineages have undergone significant diversification as they expanded; this expansion is apparently linked to a key S gene

Editor Juan E. Ludert, Center for Research and Advanced Studies (CINVESTAV-IPN)

Copyright © 2022 Lubinski et al. This is an open-access article distributed under the terms of the [Creative Commons Attribution 4.0 International license](https://creativecommons.org/licenses/by/4.0/).

Address correspondence to Javier A. Jaimes, jaj246@cornell.edu, or Gary R. Whittaker, grw7@cornell.edu.

The authors declare no conflict of interest.

Received 2 May 2022

Accepted 6 June 2022

mutation—D614G in lineage B.1 and all sublineages, which has been linked to modest increase in virus transmissibility (3) and with Q613H found in lineage A.23/A.23.1. As Q613H is adjacent to D614G, it may represent an example of convergent evolution that resulted in a more stabilized spike protein (4). D614G has now become established in circulating B and derived lineages. Compared with the lineage B.1 viruses that have successfully evolved into multiple variants of concern (VOCs), including B.1.1.7 (Alpha), B.1.351 (Beta), B.1.1.28.1/P.1 (Gamma), and B.1.617.2 (Delta), most of lineage A viruses remained at fairly lower frequency and were more prevalent at the beginning of the pandemic in Asia. However, the A.23.1 viral lineage is one of a few lineage A viruses that, due to local circumstances, became abundant in Uganda (5), Rwanda (6), and South Sudan (7). A.23.1 evolved from the A.23 virus variant first identified in Uganda in July 2020 and is characterized by three spike mutations, F157L, V367F, and Q613H (5). Subsequently, the evolving A.23.1 lineage acquired additional spike substitutions (P681R), as well as in nsp6, ORF8, and ORF9, and with the acquisition of the E484K substitution A.23.1 was designated a variant under investigation (VUI). By July 2021, the A.23.1 lineage has been observed with 1,110 genomes reported from 47 countries (GISAID, Pango Lineage report; https://cov-lineages.org/global_report_A.23.1.html).

Among several mutations in the A.23.1 lineage, the P681R mutation is of interest as it is part of a proteolytic cleavage site for furin and furin-like proteases at the junction of the spike protein receptor-binding (S1) and fusion (S2) domains (8). The S1/S2 junction of the SARS-CoV-2 S gene has a distinct indel compared to all other known SARS-like viruses (sarbecoviruses in *Betacoronavirus* lineage B); the amino acid sequence of SARS-CoV-2 S protein is ${}_{681}\text{-P-R-R-A-R}\text{-}_{686}\text{S}$ with proteolytic cleavage (|) predicted to occur between the arginine and serine residues depicted. Based on nomenclature established for proteolytic events (9), the R|S residues are defined as the P1|P1' residues for enzymatic cleavage, with residue 681 of A.23.1 spike being the P5 cleavage position. The ubiquitously-expressed cellular serine protease furin is highly specific and cleaves at a distinct multibasic motif containing paired arginine residues; furin requires a minimal motif of R-x-x-R (P4-x-x-P1), with a preference for an additional basic (B) residue at P2; i.e., R-x-B-R (10). For SARS-CoV-2, the presence of the S1/S2 "furin site" enhances virus transmissibility (11, 12). For the A.23.1 S, P681R provides an additional basic residue at P5 and may modulate S1/S2 cleavability by furin, and hence virus infection properties (13). Notably, the P681R substitution appears in several other lineages, most notably B.1.617.2 (Delta) ($n = 617,590$ genomes) but also the AY.X sublineages of B.1.617.2, B.1.617.1 ($n = 6,138$), B.1.466.2 ($n = 2,208$), the B.1.1.7 sublineage Q.4 ($n = 2,067$), B.1.551 ($n = 722$), AU.2 ($n = 302$), B.1.1.25 ($n = 509$), B.1.466.2 ($n = 538$), and other lineages (updated 22 Oct 2021; <https://outbreak.info>; <https://outbreak.info/situation-reports?pango&muts=S%3AP681R>), suggesting that the substitution may provide an advantage for viruses encoding the substitution.

We previously studied the role of proteolytic activation of the spike protein of the lineage B SARS-CoV-2 isolates Wuhan-Hu1 and B.1.1.7 (14). Here, we used a similar approach to study the role of the proteolytic activation of the spike protein in the context of the A.23.1 lineage virus, with a focus on the P681R substitution to better understand the role of this notable change at the S1/S2 (furin) cleavage site.

RESULTS

Emergence and analysis of SARS-CoV-2 variants in Uganda, and evolution of the P681R mutation and its role in the transmissibility and emergence of SARS-CoV-2.

A summary of the daily reported SARS-CoV-2 infections in Uganda is shown in Fig. 1A, along with a summary of SARS-CoV-2 lineage data in samples from Uganda (Fig. 1B). The peak of infections in December 2020–January 2021 corresponded to the circulation of the A.23.1 variant, which subsided but was replaced by a second larger peak of infections beginning in July 2021, primarily due to the emergence of the B.1.617.2 variant (Delta), with additional variants being present over time. The circulation of the A.23.1 variant appears to be fully displaced by the B.1.617.2 variant, which by July 2021 became the prevalent variant in this country.

To further understand the evolution of the P681R substitution and its role in the transmissibility of SARS-CoV-2, we monitored the frequency of substitutions at the S1/S2 (furin cleavage) site in the global surveillance data and plotted these substitution data as fraction

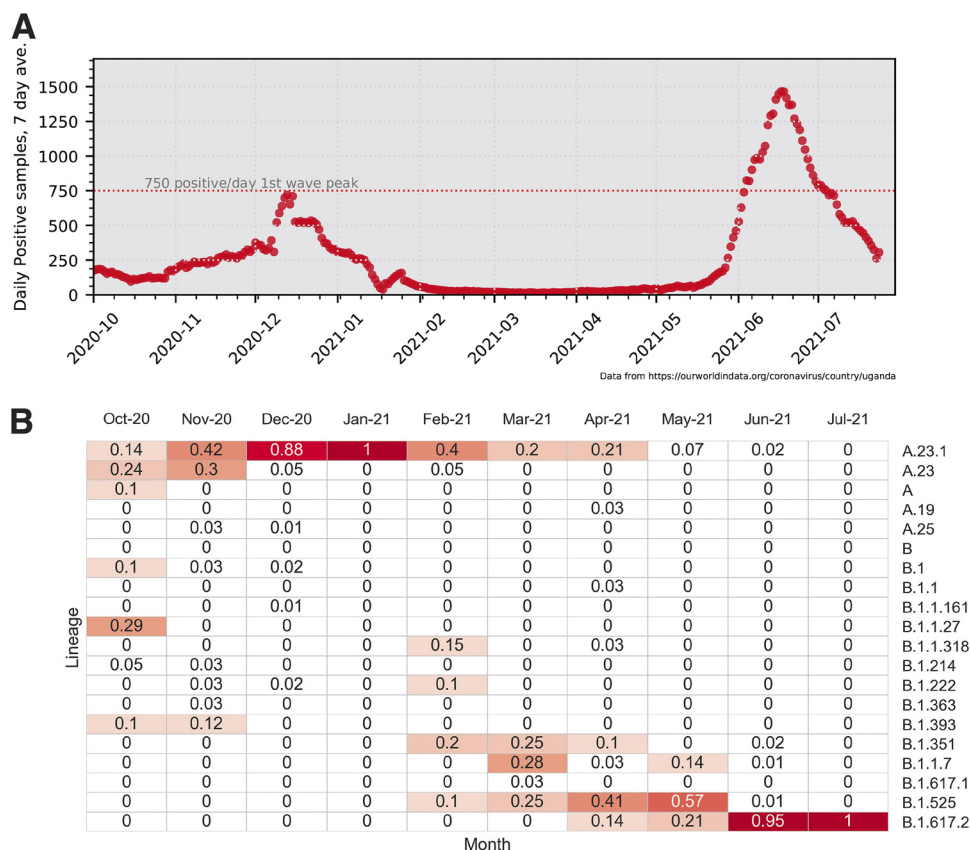


FIG 1 Uganda SARS-CoV-2 cases and lineages, October 2020 to July 2021. (A) Seven-day average positive cases numbers were plotted by day; the peak of 750 cases/per day observed in the first wave of infections in January 2021 is indicated with a dotted line. Case data were obtained from Our World in Data (<https://ourworldindata.org/>). (B) Monthly SARS-CoV-2 lineage data for Uganda. All Uganda full genome sequences from GISAID (<https://www.gisaid.org/>) were retrieved, lineage types were determined using the Pango tool (<https://cov-lineages.org/resources/pangolin.html>), and the fraction of each month's total genomes were plotted. Fractions are indicated in each cell, and cells are colored (white to dark red) by increasing fraction.

of total genomes. The initial B lineage virus that spread out of Wuhan encoded a spike protein with P681 at the furin cleavage site, along with G614. Fairly early in the epidemic, the D614G substitution appeared in the B.1 lineage and became prevalent in May–December 2020 (Fig. 2A). The B.1.1.7 (Alpha) lineage evolved from B.1, spread widely in the United Kingdom and other regions, and encoded a P681H substitution in the G614 background. B.1.1.7 peaked globally in March–April 2021 (Fig. 2A). In most regions of the world, the B.1.617.2 (Delta) lineage encoding spike D614G and P681R spread widely following its emergence in India in May–June 2021, and became the dominant observed lineage globally (Fig. 2A). In comparison, a distinct A lineage virus (A.23) containing Q613H appeared in August–September 2020 and acquired the P681R mutation at a much earlier time (December 2020–January 2021); however, it circulated only briefly (Fig. 2B). These data suggest that while P681R is important, it operates in the context of other viral mutations in the context of community spread, with this functional context able to be addressed experimentally.

Biochemical analysis of the SARS-CoV-2 A.23.1 S1/S2 cleavage site. To gain insight into SARS-CoV-2 spike protein function and the proteolytic processing at the S1/S2 site, we took a combined biochemical and cell-based strategy, with the rationale that along with other changes in the spike protein, A.23.1, B.1.617.1 (Kappa), and B.1.617.2 (Delta) contain a P681R substitution at the S1/S2 interface that may modulate spike protein function, and that these mutations alter the furin cleavage site—which can be monitored by analyzing downstream changes in the levels of cleaved products and in virus-cell fusion and pseudoparticle activation. Sequences of representative S1/S2 sequences are summarized in Fig. 3A.

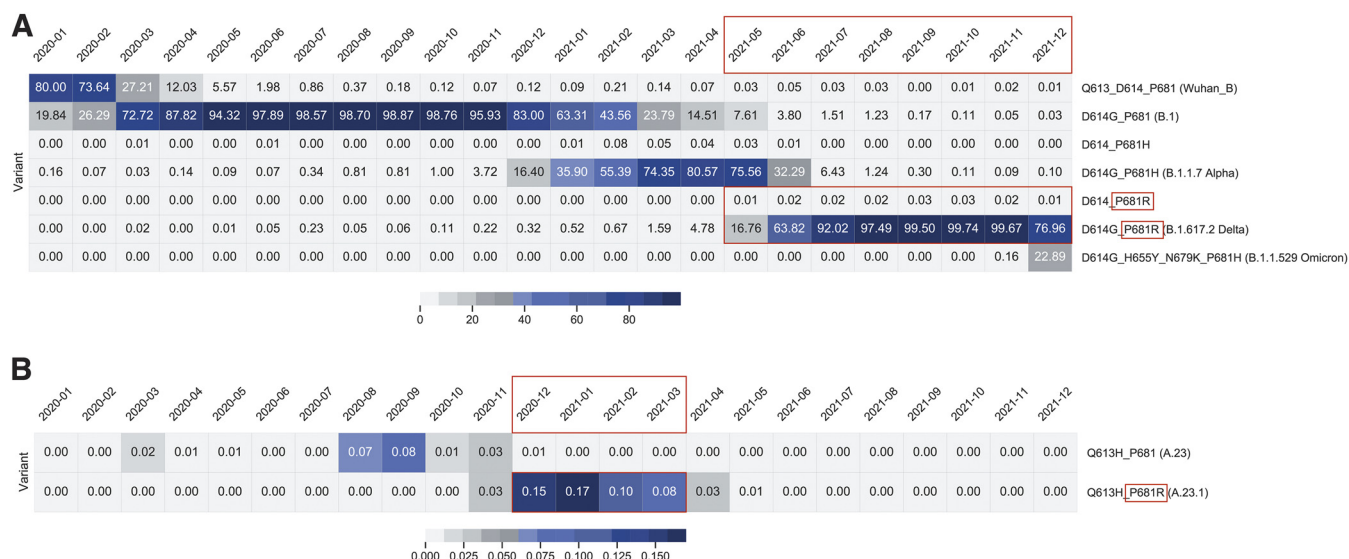


FIG 2 Frequency of P681, P681R, P681H, D614, D614G, and D613H substitutions. The frequency of substitutions was counted by string matching to a peptide sequence spanning the position 613 to 681 including the relevant sites at 613/614 and 681 (D614_P681 [Wuhan_B], D614G_P681 [B.1], D614_P681H, D614G_P681H [B.1.1.7], D614_P681R, Q613_P681 [Wuhan_B], Q613H_P681 [A.23], Q613H_P681R [A.23.1], and D614G_P681R [B.1.617.2]). Fractions of total genomes available for each month were plotted. Color bar at the bottom of each panel indicate fraction/color code. (A) Lineage A.23.1 relevant substitutions. The time periods where P681R was dominant in each lineage are shown in red boxes.

As an initial bioinformatic approach to assess biochemical function, we utilized the PiTou (15) and ProP (16) protein cleavage prediction tools, comparing the spike proteins from A.23.1 to B.1.1.7 and the prototype SARS-CoV-2 from the A.1 and B.1 lineages (e.g., Wuhan-Hu-1), as well as to MERS-CoV, and selected other human respiratory betacoronaviruses (HCoV-HKU1 and HCoV-OC43) with identifiable furin cleavage sites (Fig. 3B). Both algorithms predicted an increase in the furin cleavage for the A.23.1 and B.1.617 lineages compared to A.1/B.1, with PiTou also showing a marked increase compared to B.1.1.7. PiTou utilizes a hidden Markov model specifically targeting 20 amino acid residues surrounding furin cleavage sites and is expected to be a more accurate prediction tool. As expected, MERS-CoV showed a relatively low furin cleavage score, with HCoV-HKU1 and HCoV-OC43 showing relatively high furin cleavage scores. Overall, these analyses predict a distinct increase of furin cleavability for the spike protein of A.23.1 and B.1.617 lineage viruses compared to A.1/B.1 and B.1.1.7. lineage viruses.

To directly examine the activity of furin on the SARS-CoV-2 A.23.1 S1/S2 site, we used a biochemical peptide cleavage assay to directly measure furin cleavage activity *in vitro* (17). The specific peptide sequences used here were SARS-CoV-2 S1/S2 B.1.1.7 (TNSHRRARSVA), TNSPRRARSVA (Wuhan-Hu-1 S1/S2), and TNSRRRARSVA (A.23.1 S1/S2). As predicted, furin effectively cleaved both the Wuhan-Hu-1 (wild type; WT) and B.1.1.7 peptides, but with no significant differences (Fig. 3C). Interestingly, and agreeing with the PiTou prediction, we observed a significant increase in furin cleavage for the A.23.1 S1/S2 peptide (Fig. 2B and C) compared to both Wuhan-Hu-1 (WT) and B.1.1.7. This comparative data with SARS-CoV S1/S2 sites reveals that the P681R substitution substantially increases cleavability by furin, beyond the small increase noted previously for P681H (11).

Cell-to-cell fusion assays of A.23.1 spike. In order to assess the functional properties of the spike protein and to see if the P681R substitution provided any advantage for cell-to-cell transmission or syncytia formation, we performed a cell-to-cell fusion assay in which VeroE6 or Vero-TMPRSS2 cells were transfected with either the WT, A.23.1, or P681R spike gene. We then evaluated syncytia formation as a read-out of membrane fusion. We observed an increase in the syncytia formation following spike protein expression for either A.23.1 or Wuhan-Hu-1 harboring a P681R mutation (labeled P681R in figures), compared to Wuhan-Hu-1 (WT) (Fig. 4A). Vero-TMPRSS2 cells generally formed more extensive syncytia than VeroE6 cells. This increase was evident by observation through fluorescence microscopy, as well as

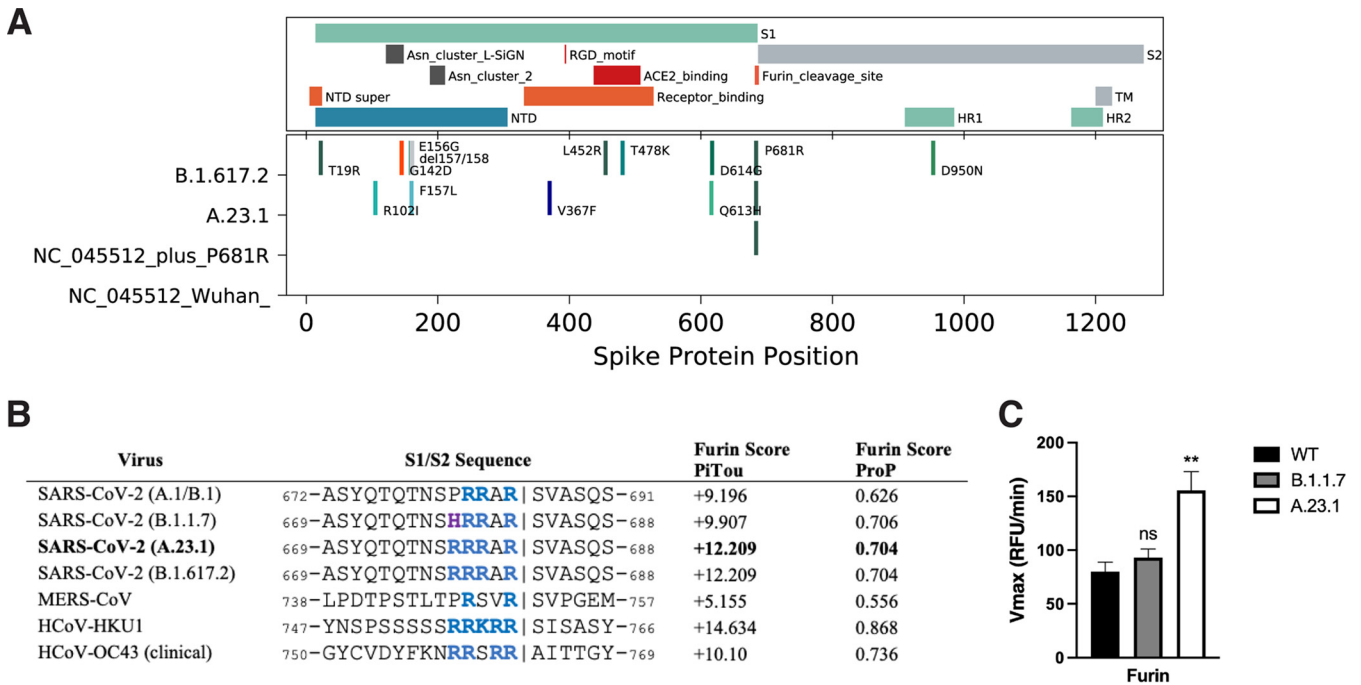


FIG 3 SARS-CoV-2 A.23.1 S sequence changes and S1/S2 furin cleavage. (A) Summary of notable functional domains and sequence changes in the spike gene of A.23.1 compared to Wuhan-Hu-1 and B.1.617.2 (Delta). (B) Furin cleavage score analysis of CoV S1/S2 cleavage sites. CoV S sequences were analyzed using the ProP1 1.0 and PiTou2 3.0 furin prediction algorithm, generating a score with bold numbers indicating predicted furin cleavage. | denotes the position of the predicted S1/S2 cleavage site. Basic residues, arginine (R) and lysine (K), are highlighted in blue, with histidine (H) in purple. Sequences corresponding to the S1/S2 region of SARS-CoV-2 (QHD43416.1), SARS-CoV (AAT74874.1), MERS-CoV (AFS88936.1), HCoV-HKU1 (AAT98580.1), and HCoV-OC43 (KY3689907.1) were obtained from GenBank. Sequences corresponding to the S1/S2 region of SARS-CoV-2 B.1.1.7 (EPI_ISL_1374509) and SARS-CoV-2 A.23.1 hCoV-19/Uganda/UG185/2020 (EPI_ISL_955136), were obtained from GISAID. (C) Fluorogenic peptide cleavage assays of the SARS-CoV-2 S1/S2 cleavage site. Peptides mimicking the S1/S2 site of the SARS-CoV-2 Wuhan-Hu-1 (WT - P681), B.1.1.7 (P681H), and A.23.1 (P681R) variants were evaluated for *in vitro* cleavage by furin, compared to trypsin control. Error bars represent G standard errors ($n = 9$). Asterisks indicate statistical significance compared to the untreated control. Statistical analysis was performed using an unpaired Student's *t* test. **, $P < 0.01$.

by quantification of the syncytia and cell-to-cell fusion ratio (Fig. 4A, B, and C). An increase in the number of nuclei involved in syncytia was observed in cells transfected with A.23.1 and P681R S genes in both cell lines (Fig. 4B) compared to WT. However, the increase was higher in Vero-TMPRSS2 cells in all the three studied spike proteins. Membrane expressed spike cleavage was also assessed using Western blot (Fig. 4C). An increased cleavage ratio was observed in the A.23.1 and P681R membrane expressed spikes, compared to WT. The cleavage ratio was similar in both cell lines. Band intensity was normalized to the GLUT4 protein (housekeeping protein) band intensity. These data provide evidence that the P681R mutation increases membrane fusion activity of the SARS-CoV-2 spike protein under the conditions tested.

Functional analysis of virus entry using viral pseudoparticles. To assess the functional importance of the S1/S2 site for SARS-CoV-2 entry, we utilized viral pseudoparticles consisting of a murine leukemia virus (MLV) core displaying a heterologous viral envelope protein to partially recapitulate the entry process of the native coronavirus. The pseudoparticles also contain a luciferase reporter gene as well as the integrase activity to allow that integration into the host cell genome to drive expression of quantifiable luciferase (MLVpp-SARS-CoV-2 S) (18). Using the HEK-293T cell line for particle production, MLV pseudoparticles containing the spike proteins of A.23.1, Wuhan-Hu-1 SARS-CoV-2 (WT), and a P681R point mutant of Wuhan-Hu-1 (P681R) were prepared. Positive-control particles containing the vesicular stomatitis virus (VSV) G protein and negative-control particles (Δ envpp) lacking envelope proteins were also prepared (not shown). Pseudoparticles were probed for their S content via Western blot (Fig. 5A). Because SARS-CoV-2 S has an efficiently cleaved spike we also produced particles under furin inhibition using dec-RVKR-CMK. This allowed changes in cleavage patterns between different spike proteins to be visualized. We also treated the particles with exogenous furin (+ or - furin) to examine the spike cleavage on both partially cleaved and uncleaved

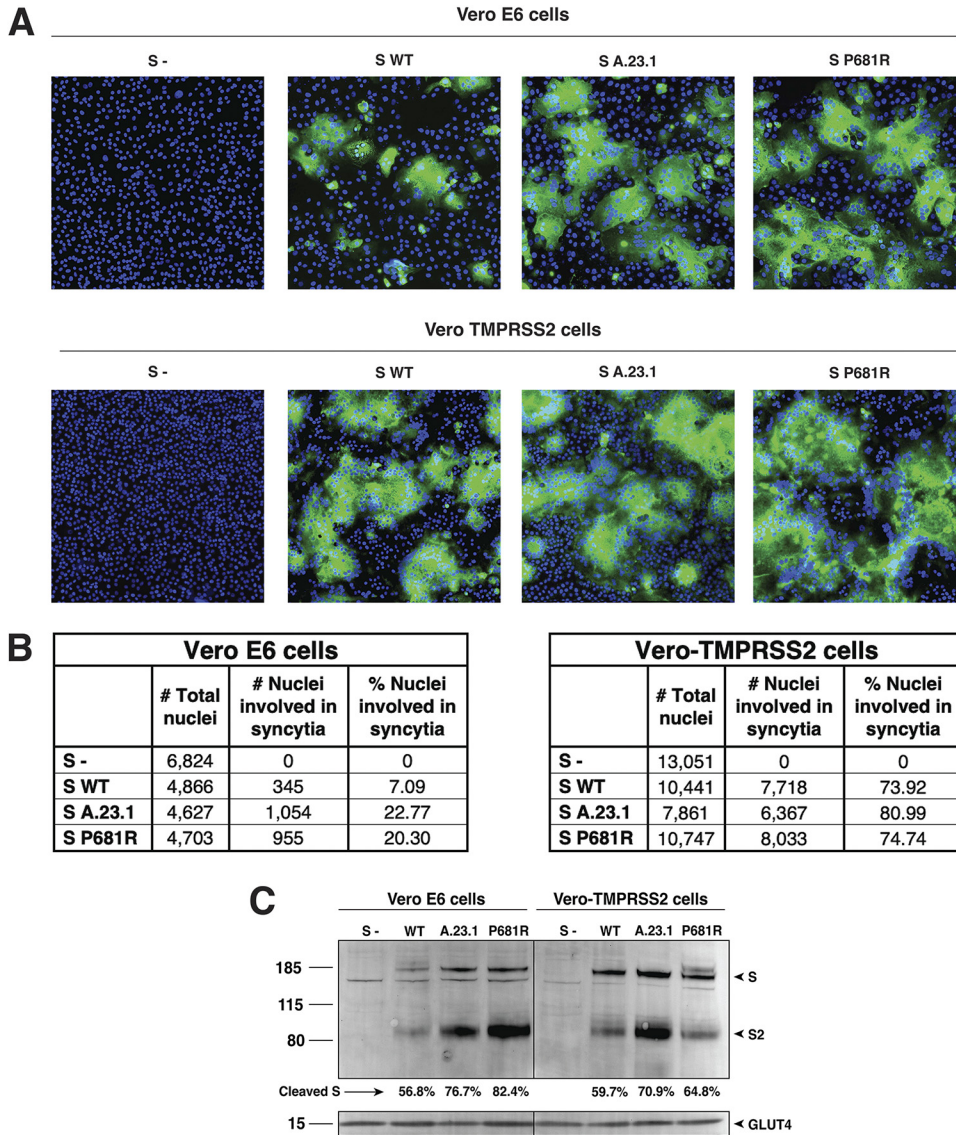


FIG 4 Cell-to-cell fusion in SARS-CoV-2 A.23.1 S expressing cells. (A) Cell-to-cell fusion assay of SARS-CoV-2 Wuhan-Hu-1 S (WT), SARS-CoV-2 S A.23.1 variant, or SARS-CoV-2 S WT with P681R mutation. S-, non-transfected cells. SARS-CoV-2 S was detected using a rabbit antibody against the SARS-CoV-2 S2 region. (B) Syncytia quantification by number of nuclei involved in syncytia. (C) Western blot analysis of membrane expressed S proteins and GLUT4 (housekeeping expression protein). All of the experiments were performed on Vero E6 and Vero-TMPRSS2 cells.

spikes, to further study the differences in furin processing in the studied spikes. For both A.23.1 and P681R particles, we detected increased spike protein cleavage compared to WT in the harvested particles (Fig. 5A). Interestingly, we observed markedly increased cleavage ratio for both A.23.1 and P681R spikes in the harvested pseudoparticles under furin-inhibition conditions (Fig. 5A), presumably as the enhanced furin cleavage motif site produced by the P681R mutation rescued what may be a modest effect of dec-RVKR-CMK.

For SARS-CoV-2, furin is predicted to cleave during virus assembly and “prime” the spike protein at the S1/S2 site for subsequent events during cell entry. However, a subsequent cleavage priming at a secondary site (known as S2’ site) is also needed to activate the spike’s fusion machinery (1). SARS-CoV-2 is predicted to enter Vero E6 cells using cathepsin L for activation during endosomal trafficking, in what is known as the “late” pathway, whereas in Vero-TMPRSS2 is predicted to use a “early” pathway, with spike activated by TMPRSS2 or other transmembrane serine proteases (TTSPs) at the cellular membrane (1). Here, we used the Vero-TMPRSS2 and the Vero E6 cell lines, which are predicted to activate the

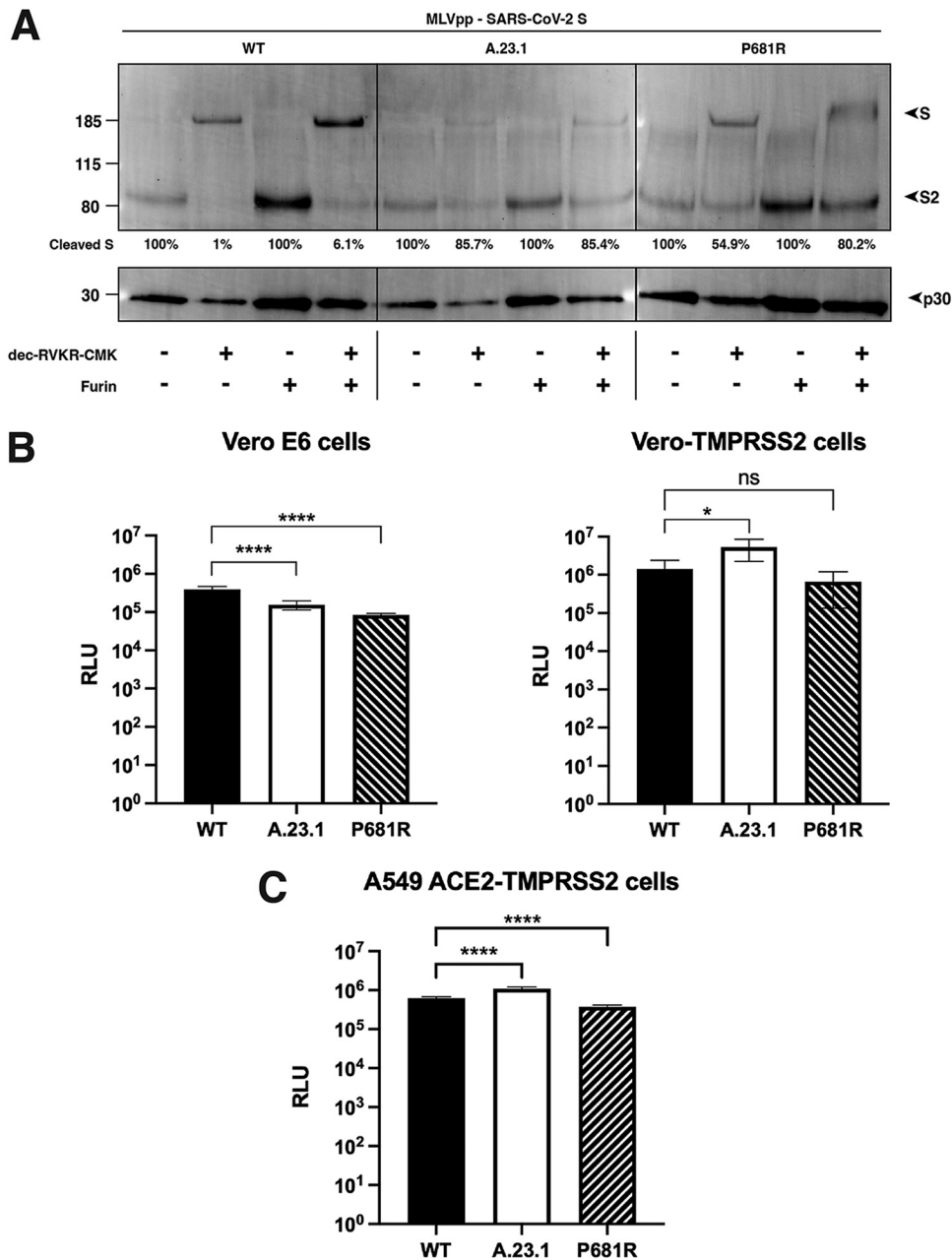


FIG 5 SARS-CoV-2 A.23.1 variant S1/S2 cleavage site activation and role in viral entry. (A) Western blot analysis of MLVpp-SARS-CoV-2 S produced in \pm dec-RVKR-CMK and treated with \pm furin. S was detected using a rabbit antibody against the SARS-CoV-2 S2 subunit. MLV content was detected using a mouse antibody against MLV p30. (B) Pseudoparticle infectivity assays in Vero E6 and Vero-TMPRSS2 cells. Cells were infected with MLVpps harboring the SARS-CoV-2 S (WT), SARS-CoV-2 S A.23.1 variant, and SARS-CoV-2 S WT with P681R mutation. Data represent the average luciferase activity of cells of four independent experiments (Vero E6 and Vero-TMPRSS2). Error bars represent G standard deviation ($n = 4$). Asterisks indicate statistical significance compared to the untreated control. Statistical analysis was performed using an unpaired Student's t test. *, $P < 0.1$; ****, $P < 0.0001$. (C) Pseudoparticle infectivity assays in A549-ACE2-TMPRSS2 cells. Cells were infected with MLVpps harboring the SARS-CoV-2 S (WT), SARS-CoV-2 S A.23.1 variant, and SARS-CoV-2 S WT with P681R mutation. Data represent the average luciferase activity of cells of three independent experiments. Error bars represent G standard deviation ($n = 3$). Asterisks indicate statistical significance compared to the untreated control. Statistical analysis was performed using an unpaired Student's t test. ****, $P < 0.0001$.

SARS-CoV-2 using TMPRSS2 and cathepsin L, respectively. Considering that furin priming at the S1/S2 site normally occurs during viral assembly, we used pseudoparticles that were produced without furin inhibitor, yielding cleaved spike proteins. Vero-TMPRSS2 cells gave overall significantly higher luciferase signals indicative of more efficient entry. In contrast, Vero E6 cells showed generally lowered infection levels. As expected, VSVpp

(positive control) pseudoparticles infected both cell lines with several orders of magnitude higher luciferase units than the values reported with $\Delta envpp$ infection (data not shown). In Vero E6 cells, entry of A.23.1. and P681R was lowered compared to wild type (Fig. 5B). However, Vero-TMPRSS2 cells pseudoparticles bearing the A.23.1 spike showed a significantly higher level of infection, indicating more efficient virus entry. This was not reproduced for a P681R point mutant of Wuhan-Hu-1 (P681R), a result in line with previous results indicating that other mutations in spike are needed for the increased cleavability imparted by the P681R mutation to mediate enhanced virus infection.

As a further way to assess the entry mediated by A.23.1. and P681R-containing spike proteins, we tested pseudoparticles in human lung A459 cells expressing ACE2 and TMPRSS2 (Fig. 5C). These cells showed a highly significant increase in infection by A.23.1 compared to Wuhan-Hu1. The point mutant of P681R on the Wuhan-Hu1 background showed a decrease in infectivity, confirming that P681R (similarly to other point mutants [19]) only has its functional consequence on the appropriate genetic background.

DISCUSSION

Since late 2020, the evolution of the SARS-CoV-2 pandemic has been characterized by the emergence of viruses bearing sets of substitutions/deletions, designated “variants of concern” (VOCs) and “variants under investigation” (VUIs). These variants appear to have expanded following the selection for substitution or deletions in the spike protein, such as D614G and Q613H, along with mutations in other viral proteins. The substitutions encoded by such variants may alter virus characteristics including enhanced transmissibility and antigenicity, and some provide a direct advantage to avoid the changing developing immune responses in the population due to prior exposure or vaccination as well as the social dynamics of the human population (4, 20–23). The specific case of the D614G is interesting, as this mutation has been shown to improve the spike’s open conformation for receptor binding, demonstrating an evolutionary advantage for the 614G carrier virus (24). In fact, the explosive spread of COVID-19 cases can be traced to the emergence of this mutation, which provided the context for further evolution of the SARS-CoV-2 virus and the rising number of new variants. The first notable SARS-CoV-2 VOC of 2021 was B.1.1.7 (Alpha), which, among other changes, encoded a P681H substitution in the spike S1/S2 furin cleavage site and has been linked to increased transmissibility due to the presence of the additional basic amino acid, histidine (H). However, histidine is unusual in that it has an ionizable side chain with a pKa near neutrality (25), and so is not conventionally considered a basic amino acid. Most recently, the VOC (B.1.617.2, or Delta) has replaced B.1.1.7 (Alpha) as the dominant circulating virus globally, which, like A.23.1 and sublineages B.1.617.1, B.1.617.2, and B.1.617.3, encodes a P681R substitution and is more conventionally “polybasic” in the S1/S2 cleavage motif than the P681H of B.1.1.7 (Alpha) and is suggested to affect transmissibility and pathogenesis (26). For the Delta variant (B.1.617.2), Saito et al. (26) showed enhanced fusogenicity and viral entry in cells expressing TMPRSS2 (Vero-TMPRSS2 and Calu-3) but lowered fusogenicity in Vero E6 cells (27), with equivalent results also shown by Peacock et al. in a range of TMPRSS2-expressing cells (28). Our data with Vero E6 cells in particular differ from those reported by Saito et al., reinforcing the concept that cell–cell fusion can be affected by many factors, including the specific growth conditions of the cells, and also suggesting that other mutations in the A.23.1 spike specifically affect fusion in non-TMPRSS2-expressing cells. Interestingly, another study, by Rajah et al., showed increased syncytia formation in U2OS-ACE2 and Vero E6 cells infected with Alpha and Beta variants compared to Wuhan-Hu-1 and D614G (29). However, the syncytia formation in Vero E6 cells was significantly lower, compared to U2OS-ACE2.

The A.23.1 variant predated the B.1.617 lineage as a P681R-containing VOC/VOI by several months. It is interesting to note that B.1.617.2 (Delta) has been shown to be a genetic outlier compared to other VOCs (30), raising the question of whether P681R (found in A.23.1 and B.1.617) ultimately results in a more successful viral variant compared to P681H, found in B.1.1.7 (Alpha) and B.1.529 (Omicron BA.1/BA.2). A recent study has shown that reverting the P681R mutation to either P681H or WT P681 in the context of the Delta

variant, significantly reduced the replication of the virus in cell culture (31), therefore emphasizing the importance of this mutation for the enhanced replication phenotype of Delta.

It is important to note that both lineages that have temporarily dominated Uganda have encoded the spike P681R substitution, but in combination with distinct changes in the spike protein. In all cases, the position 681 change occurred after a change of position 613/614 (B to B.1 to B.1.1.7 [Alpha], B to B.1 to B.1.617.2 [Delta], A to A.23 to A.23.1, B to B.1 to B.1.1.7 to Q.4), and most recently B to B.1 to B.1.1.529 (Omicron). This timing and linkage can be seen in the lineage prevalence charts (Fig. 5A and B), where for each major lineage the position 613/614 changes predate the position 681 changes.

The analyses reported here show that the substitution influences furin-mediated cleavage at the *in vitro* level, with these results being consistent with other studies (22, 23). However, P681R may not be the sole driver of spike protein function *in vivo*—a finding reinforced by the molecular studies described here. It would be of interest to understand the additional spike-associated changes that cooperate with P681R. The introduction of P681R alone into the WT Wuhan-Hu-1 spike did not reproduce the full activity of the A.23.1 spike (Fig. 3 and 4). This contrasts with a recent report by Kuzmina et al., where the introduction of the P681H or the P681R mutation resulted in increased fusion (32). However, it is unclear if these mutations were introduced in the context of the D614 or the D614G mutation. One limitation of this study is that isolated viruses of the A.23.1 lineage are not available for infectivity assays, and so our work relies on the use of epidemiological tools and the reconstruction of virus infection in biochemical and cell-based assays. Another limitation is that our “wild-type” B lineage virus contains D614 and not 614G. Despite these limitations, we consider that our data support our conclusion that the spike mutation P681R—by itself—is not a primary driver of virus transmissibility in the population, with A.23.1 giving unique insight into these aspects of the ongoing COVID-19 pandemic, but requires the full context of additional spike and other viral changes seen in A.23.1, B.1.617.2, and Q.4 for transmission success.

A.23.1 was a key SARS-CoV-2 variant spreading within Africa during the early part of 2021, and has been defined (along with C.11) as an African VOI (33) having multiple mutations on the spike glycoprotein and evolving in a clocklike manner along with other variants. Epidemiological data from Uganda support the importance of the P681R substitution in A.23.1 for community-wide transmission. The subsequent decline of the P681R lineage A.23.1 in Uganda, combined with the *in vitro* analyses reported here, clearly showed that the P681R alone is not sufficient to drive such dominance. The P681R lineage B.1.617.2 (Delta) likely benefited from additional S and other substitutions and eventually dominated the Uganda epidemic by June 2021 (Fig. 5), similar to patterns globally.

While P681R does make the S1/S2 cleavage site more basic in nature, such variant cleavage sites are still not “ideal” for furin—as originally found in the prototype furin-cleaved virus mouse hepatitis virus (MHV) (RRARR|S) (26, 34). The introduction of an arginine residue did appear to be making S1/S2 more “polybasic” as the pandemic continued and transmissibility increased. While we should not oversimplify the complex process of spike protein activation, it will be interesting to see whether this progression of basic residue addition continues with future variants, toward that seen in established community-acquired respiratory coronaviruses such as HCoV-HKU-1 or HCoV-OC43, with S1/S2 sequences of RRKRR|S and RRSRR|A, respectively (26). The recent emergence of B.1.1.529 (Omicron), without P681R but containing distinct changes in its S1/S2 cleavage site (N579K, P681H) and apparently distinct properties in regard to spike protein antigenicity, protease activation, and fusion (for example, see reference 35), has reaffirmed the notion that the coronavirus spike protein is highly adaptable.

MATERIALS AND METHODS

Cells. All cell lines: Vero E6 (ATCC CRL-1586), HEK-293T (ATCC CRL-3216), Vero-TMPRSS2 cells (JCRB Cell Bank JCRB1819), and A549-ACE2-TMPRSS2 cells (Invivogen a549-hace2tps) were grown according to the manufacturer's instructions.

Furin prediction calculations. ProP: CoV sequences were analyzed using the ProP 1.0 server hosted at <https://services.healthtech.dtu.dk/service.php?ProP-1.0>. PiTou: CoV sequences were analyzed using the PiTou V3 software (15).

Fluorogenic peptide assays. Fluorogenic peptide assays were performed as described previously in reference 36. Peptides SARS-CoV-2 S1/S2 Wuhan-Hu-1 (WT) (TNSPRRARSVA), SARS-CoV-2 S1/S2

B.1.1.7 (TNSHRRARSVA), and SARS-CoV-2 S1/S2 A.23.1 (TNSRRRARSVA) were obtained from Biomatik USA, LLC.

Plasmids. The sequence for the A.23.1 spike gene from isolate SARS-CoV-2 A.23.1 hCoV-19/Uganda/UG185/2020 (EPI_ISL_955136) was obtained from GISAID (<https://www.gisaid.org/>), codon-optimized, synthesized, and cloned into a pcDNA 3.1+ vector for expression (GenScript). pcDNA 3.1+ plasmid harboring the Wuhan-Hu-1 spike was generously provided by David Veessler, University of Washington, United States. Site-directed mutagenesis was carried out on the Wuhan-Hu-1 S plasmid using the Agilent QuikChange Lightning Mutagenesis kit.

Cell-cell fusion assay. Vero E6 and Vero-TMPRSS2 cells were transfected with a plasmid harboring the spike gene of the SARS-CoV-2 Wuhan-Hu-1 S (WT), SARS-CoV-2 A.23.1 S, SARS-CoV-2 Wuhan-Hu-1 with a P681R mutation, or an empty pcDNA3.1+ (S-) and evaluated for syncytia formation through an immunofluorescence assay (IFA). Transfection was performed using Lipofectamine 3000 (cat.: L3000075, Invitrogen Co.), following the manufacturer's instructions. Syncytia were visualized through fluorescence microscopy using a previously described method (14). The spike expression was detected using a SARS-CoV-2 spike antibody (cat.: 40591-T62, Sino Biological, Inc.). Images were taken at 20× on the Echo Revolve fluorescence microscope (model: RVL-100-M). Nuclei were counted manually using the Cell Counter plugin in ImageJ (<https://imagej.nih.gov/ij/>). Cells that expressed the spike protein and contained 4 or more nuclei were considered to be one syncytium.

Cell surface expression of spike protein. Vero E6 and Vero TMPRSS2 cells were transfected with SARS-CoV-2 Wuhan-Hu-1 S (WT), SARS-CoV-2 A.23.1 S, SARS-CoV-2 Wuhan-Hu-1 with a P681R mutation, or an empty pcDNA3.1+ (S-) using polyethylenimine (PEI) and incubated for 24 h. Membrane-bound expressed protein was analyzed through a cell surface biotinylation assay and a Western blot as described previously (37). The spike expression was detected using a SARS-CoV-2 spike antibody (cat.: 40591-T62, Sino Biological, Inc.). GLUT4 protein was used as a housekeeping expression control and labeled using a GLUT4 monoclonal antibody (cat.: MA5-17175, Invitrogen Co.). S expression was normalized to the GLUT4 housekeeping control. Then, the S cleavage ratio quantification was performed by comparing the normalized band intensity to the cleaved band intensity, and using the formula $(S2/(S+S2)) \times 100$. Quantification and ratio calculations were performed using ImageJ (<https://imagej.nih.gov/ij/>).

Pseudoparticle generation and infection assays. Pseudoparticle generation was carried out using a murine leukemia virus (MLV)-based system as previously described with minor modifications (14, 18). Briefly, HEK-293T cells were transfected with 800 ng of pCMV-MLV *gag-pol*, 600 ng of pTG-Luc, and 600 ng of a plasmid containing the viral envelope protein of choice. Viral envelope plasmids included pcDNA-SARS-CoV-2 Wuhan-Hu-1 S as the WT, and pcDNA-SARS-CoV-2 Wuhan-Hu-1 P681R S, and pcDNA-SARS-CoV-2 A.23.1 S. pCAGGS-VSV G was used as a positive control and pCAGGS3.1+ was used for an empty plasmid negative control (S-). Transfection was performed using polyethylenimine (PEI) as described previously. Forty-eight h posttransfection, the supernatant containing the pseudoparticles was removed, centrifuged to remove cell debris, filtered, and stored at -80°C. Pseudoparticle infection assays were performed as previously described, with minor adjustments (18).

Western blot analysis of pseudoparticles. A 3-mL volume of pseudoparticles was pelleted using a TLA-55 rotor with an Optima-MAX-E ultracentrifuge (Beckman Coulter) for 2 h at 42,000 rpm at 4°C. Untreated particles were resuspended in 30 μL DPBS buffer. Pseudoparticles were generated as described in the pseudoparticle generation section, with the furin inhibitor dec-RVKR-CMK (cat.: 35-011, Tocris) being added during transfection to select wells. For the + furin treated MLVpps, particles were resuspended in 30 μL of furin buffer consistent in 20 mM HEPES, 0.2 mM CaCl₂, and 0.2 mM β-mercaptoethanol (at pH 7.0). Furin-treated particles were later incubated with 6 U of recombinant furin for 3 h at 37°C. Sodium dodecyl sulfate (SDS) loading buffer and DTT were added to all samples and heated at 95°C for 10 min. Samples were separated on NuPAGE Bis-Tris gel (Invitrogen) and transferred on polyvinylidene difluoride membranes (GE). SARS-CoV-2 S was detected using a rabbit polyclonal antibody against the S2 domain (cat.: 40590-T62, Sinobiological). Bands were detected using the ChemiDoc Imaging software (Bio-Rad), and band intensity was calculated using the analysis tools on Bio-Rad Image Lab 6.1 software to determine the uncleaved to cleaved S ratios.

Uganda cases versus viral lineages over time. For daily reported SARS-CoV-2 infections, the Uganda daily SARS-CoV-2 positive samples numbers were retrieved from Our World in Data (<https://ourworldindata.org/coronavirus>), and the 7-day average was determined. Uganda SARS-CoV-2 lineage data were generated from the MRC Uganda genomic data deposited in the GISAID database (<https://www.gisaid.org/>). SARS-CoV-2 Pango lineages (2) were determined using the pangolin module pangoleARN (<https://github.com/cov-lineages/pangolin>).

Spike position 681 and 613/614 changes in global data. All available spike protein sequences were obtained from the GISAID database. The frequency of P681, P681R, P681H, D614, D614G, and D613H were counted by string matching using Ack (<http://beyondgrep.com/>) with the major variations of the 88 amino acid peptide sequence (amino acids 605 to 691) spanning the two relevant sites [D614_P681 (Wuhan_B), D614G_P681 (B.1), D614_P681H, D614G_P681H (B.1.1.7), D614_P681R, Q613_P681 (Wuhan_B), Q613H_P681 (A.23), Q613H_P681R (A.23.1), and D614G_P681R (B.1.617.2)]. Fractions of available total genomes for each month encoding each peptide variant were visualized in a heatmap. Additional changes at position H655Y (present in the Gamma lineage) were also included in the count and fraction calculation, but the total numbers were minor.

Quantification and statistical analysis. All statistical analysis was performed using GraphPad Prism for Mac OS X, GraphPad Software, San Diego, California USA, www.graphpad.com. Two sample *t* tests were used to compare SARS-CoV-2 Wuhan-Hu 1 to SARS-CoV-2 A.23.1 or SARS-CoV-2 P681R, with significant *P* values reported in the figure legends. Standard deviation was calculated and included in graphs when appropriate.

SUPPLEMENTAL MATERIAL

Supplemental material is available online only.

SUPPLEMENTAL FILE 1, PDF file, 0.1 MB.

ACKNOWLEDGMENTS

This work was funded in part by the National Institute of Health research grant R01AI35270 (to G.R.W. and S.D.). We thank the global SARS-CoV-2 sequencing groups for their open and rapid sharing of sequence data and GISAID for providing an effective platform to make these data available. D.L.B., M.V.T.P., and M.C. were funded by the UK Medical Research Council (MRC/UK Research and Innovation) and the UK Department for International Development (DFID) under the MRC/DFID Concordat agreement (grant agreement no. MC_PC_20010) and Wellcome Trust, UK FCDO—Wellcome Epidemic Preparedness—Coronavirus (grant agreement no. 220977/Z/20/Z). T.T. was supported by the National Science Foundation Graduate Research Fellowship Program under grant no. DGE-1650441 and the Samuel C. Fleming Family Graduate Fellowship.

Conceptualization: B.L., L.E.F., T.T., S.D., J.A.J., and G.R.W. Methodology: B.L., L.E.F., M.V.T.P., D.L.B., J.L.C., T.T., S.D., M.C., J.A.J., and G.R.W. Investigation: B.L., L.E.F., M.V.T.P., D.L.B., J.L.C., T.T., J.A.J. Writing—Original Draft: B.L., T.T., J.A.J., and G.R.W. Writing—Review & Editing: B.L., M.V.T.P., T.T., S.D., M.C., J.A.J., and G.R.W. Visualization: B.L., L.E.F., M.V.T.P., T.T., and J.A.J. Supervision: S.D., M.C., J.A.J., and G.R.W. Funding acquisition: S.D., M.C., and G.R.W.

We declare no conflicts of interest.

REFERENCES

- Whittaker GR, Daniel S, Millet JK. 2021. Coronavirus entry: how we arrived at SARS-CoV-2. *Curr Opin Virol* 47:113–120. <https://doi.org/10.1016/j.coviro.2021.02.006>.
- Rambaut A, Holmes EC, O'Toole Á, Hill V, McCrone JT, Ruis C, Du Plessis L, Pybus OG. 2020. A dynamic nomenclature proposal for SARS-CoV-2 lineages to assist genomic epidemiology. *Nat Microbiol* 5:1403–1407. <https://doi.org/10.1038/s41564-020-0770-5>.
- Zhou B, Thao TTN, Hoffmann D, Taddeo A, Ebert N, Labrousseau F, Pohlmann A, King J, Steiner S, Kelly JN, Portmann J, Halwe NJ, Ulrich L, Trüb BS, Fan X, Hoffmann B, Wang L, Thomann L, Lin X, Stalder H, Pozzi B, de Brot S, Jiang N, Cui D, Hossain J, Wilson MM, Keller MW, Stark TJ, Barnes JR, Dijkman R, Jores J, Benarafa C, Wentworth DE, Thiel V, Beer M. 2021. SARS-CoV-2 spike D614G change enhances replication and transmission. *Nature* 592:122–127. <https://doi.org/10.1038/s41586-021-03361-1>.
- Harvey WT, Carabelli AM, Jackson B, Gupta RK, Thomson EC, Harrison EM, Ludden C, Reeve R, Rambaut A, Peacock SJ, Robertson DL, Consortium C-GU, COVID-19 Genomics UK (COG-UK) Consortium. 2021. SARS-CoV-2 variants, spike mutations and immune escape. *Nat Rev Microbiol* 19:409–424. <https://doi.org/10.1038/s41579-021-00573-0>.
- Bugembe DL, Phan MVT, Ssewanyana I, Semanda P, Nansumba H, Dhaala B, Nabadda S, O'Toole ÁN, Rambaut A, Kaleebu P, Cotten M. 2021. Emergence and spread of a SARS-CoV-2 lineage A variant (A.23.1) with altered spike protein in Uganda. *Nat Microbiol* 6:1094–1101. <https://doi.org/10.1038/s41564-021-00933-9>.
- Butera Y, Mukantwari E, Artesi M, Umuringa J. d, O'Toole ÁN, Hill V, Rooke S, Hong SL, Dellicour S, Majyambere O, Bontems S, Boujemla B, Quick J, Resende PC, Loman N, Umumarungu E, Kabanda A, Murindahabi MM, Tuyisenge P, Gashogu M, Rwabihama JP, Sindayiheba R, Gikic D, Souopgui J, Ndifon W, Rutayisire R, Gatara S, Mpunga T, Ngamije D, Bours V, Rambaut A, Nsanzimana S, Baele G, Durkin K, Mutesa L, Rujeni N. 2021. Genomic sequencing of SARS-CoV-2 in Rwanda reveals the importance of incoming travelers on lineage diversity. *Nat Commun* 12:5705. <https://doi.org/10.1038/s41467-021-25985-7>.
- Bugembe DL, Phan MVT, Abias AG, Ayei J, Deng LL, Lako RLL, Rumunu J, Kaleebu P, Wamala JF, Hm JJ, Lodiogon DK, Bunga S, Cotten M. 2021. SARS-CoV-2 variants, South Sudan, January–March 2021. *Emerg Infect Dis* 27:3133–3136. <https://doi.org/10.3201/eid2712.211488>.
- Jaimes JA, Andre NM, Chappie JS, Millet JK, Whittaker GR. 2020. Phylogenetic analysis and structural modeling of SARS-CoV-2 spike protein reveals an evolutionary distinct and proteolytically sensitive activation loop. *J Mol Biol* 432:3309–3325. <https://doi.org/10.1016/j.jmb.2020.04.009>.
- Polgár L. 1989. General aspects of proteases, p 43–86. *In* Mechanisms of protease action. CRC Press, Boca Raton, FL.
- Seidah NG, Prat A. 2012. The biology and therapeutic targeting of the proprotein convertases. *Nat Rev Drug Discov* 11:367–383. <https://doi.org/10.1038/nrd3699>.
- Johnson BA, Xie X, Bailey AL, Kalveram B, Lokugamage KG, Muruato A, Zou J, Zhang X, Juelich T, Smith JK, Zhang L, Bopp N, Schindewolf C, Vu M, Vanderheiden A, Winkler ES, Swetnam D, Plante JA, Aguilar P, Plante KS, Popov V, Lee B, Weaver SC, Suthar MS, Routh AL, Ren P, Ku Z, An Z, Debbink K, Diamond MS, Shi P-Y, Freiberg AN, Menachery VD. 2021. Loss of furin cleavage site attenuates SARS-CoV-2 pathogenesis. *Nature* 591:293–299. <https://doi.org/10.1038/s41586-021-03237-4>.
- Peacock TP, Goldhill DH, Zhou J, Baillon L, Frise R, Swann OC, Kugathasan R, Penn R, Brown JC, Sanchez-David RY, Braga L, Williamson MK, Hassard JA, Staller E, Hanley B, Osborn M, Giacca M, Davidson AD, Matthews DA, Barclay WS. 2020. The furin cleavage site of SARS-CoV-2 spike protein is a key determinant for transmission due to enhanced replication in airway cells. *bioRxiv* <https://doi.org/10.1101/2020.09.30.318311>.
- Hoffmann M, Kleine-Weber H, Schroeder S, Kruger N, Herrler T, Erichsen S, Schiergens TS, Herrler G, Wu NH, Nitsche A, Muller MA, Drosten C, Pohlmann S. 2020. SARS-CoV-2 cell entry depends on ACE2 and TMPRSS2 and is blocked by a clinically proven protease inhibitor. *Cell* 181:P271–280.e8. <https://doi.org/10.1016/j.cell.2020.02.052>.
- Lubinski B, Fernandes MHV, Frazier L, Tang T, Daniel S, Diel DG, Jaimes JA, Whittaker GR. 2022. Functional evaluation of the P681H mutation on the proteolytic activation of the SARS-CoV-2 variant B.1.1.7 (Alpha) spike. *iScience* 25:103589. <https://doi.org/10.1016/j.isci.2021.103589>.
- Tian S, Huajun W, Wu J. 2012. Computational prediction of furin cleavage sites by a hybrid method and understanding mechanism underlying diseases. *Sci Rep* 2:261. <https://doi.org/10.1038/srep00261>.
- Duckert P, Brunak S, Blom N. 2004. Prediction of proprotein convertase cleavage sites. *Protein Eng Des Sel* 17:107–112. <https://doi.org/10.1093/protein/gzh013>.
- Jaimes JA, Millet JK, Whittaker GR. 2020. Proteolytic cleavage of the SARS-CoV-2 spike protein and the role of the novel S1/S2 site. *iScience* 23:101212. <https://doi.org/10.1016/j.isci.2020.101212>.
- Millet JK, Tang T, Nathan L, Jaimes JA, Hsu HL, Daniel S, Whittaker GR. 2019. Production of pseudotyped particles to study highly pathogenic coronaviruses in a biosafety level 2 setting. *J Vis Exp* 145:e59010. <https://doi.org/10.3791/59010>.
- Goodman LB, Whittaker GR. 2021. Public health surveillance of infectious diseases: beyond point mutations. *Lancet Microbe* 2:e53–e54. [https://doi.org/10.1016/S2666-5247\(21\)00003-3](https://doi.org/10.1016/S2666-5247(21)00003-3).

20. Müller NF, Wagner C, Frazar CD, Roychoudhury P, Lee J, Moncla LH, Pelle B, Richardson M, Ryke E, Xie H, Shrestha L, Addetia A, Rachleff VM, Lieberman NAP, Huang M-L, Gautom R, Melly G, Hiatt B, Dykema P, Adler A, Brandstetter E, Han PD, Fay K, Ilcin M, Lacombe K, Sibley TR, Truong M, Wolf CR, Boeckh M, Englund JA, Famulare M, Lutz BR, Rieder MJ, Thompson M, Duchin JS, Starita LM, Chu HY, Shendure J, Jerome KR, Lindquist S, Greninger AL, Nickerson DA, Bedford T. 2021. Viral genomes reveal patterns of the SARS-CoV-2 outbreak in Washington State. *Sci Transl Med* 13:eabf0202. <https://doi.org/10.1126/scitranslmed.abf0202>.
21. Richard D, Shaw LP, Lanfear R, Corbett-Detig R, Hinrichs A, McBroome J, Turakhia Y, Acman M, Owen CJ, Tan CCS, van Dorp L, Balloux F. 2021. A phylogeny-based metric for estimating changes in transmissibility from recurrent mutations in SARS-CoV-2. *bioRxiv* <https://doi.org/10.1101/2021.05.06.442903>.
22. Grubaugh ND, Hodcroft EB, Fauver JR, Phelan AL, Cevik M. 2021. Public health actions to control new SARS-CoV-2 variants. *Cell* 184:1127–1132. <https://doi.org/10.1016/j.cell.2021.01.044>.
23. Peacock TP, Penrice-Randal R, Hiscox JA, Barclay WS. 2021. SARS-CoV-2 one year on: evidence for ongoing viral adaptation. *J General Virology* 102:001584. <https://doi.org/10.1099/jgv.0.001584>.
24. Yurkovetskiy L, Wang X, Pascal KE, Tomkins-Tinch C, Nyalile TP, Wang Y, Baum A, Diehl WE, Dauphin A, Carbone C, Veinotte K, Egri SB, Schaffner SF, Lemieux JE, Munro JB, Rafique A, Barve A, Sabeti PC, Kyratsous CA, Dudkina NV, Shen K, Luban J. 2020. Structural and functional analysis of the D614G SARS-CoV-2 spike protein variant. *Cell* 183:739–751.e8. <https://doi.org/10.1016/j.cell.2020.09.032>.
25. Nelson DL, Cox MM. 2000. *Lehninger principles of biochemistry*. Worth Publishers.
26. Whittaker GR. 2021. SARS-CoV-2 spike and its adaptable furin cleavage site. *Lancet Microbe* 2:e488–e489. [https://doi.org/10.1016/S2666-5247\(21\)00174-9](https://doi.org/10.1016/S2666-5247(21)00174-9).
27. Saito A, Irie T, Suzuki R, Maemura T, Nasser H, Uriu K, Kosugi Y, Shirakawa K, Sadamasu K, Kimura I, Ito J, Wu J, Iwatsuki-Horimoto K, Ito M, Yamayoshi S, Loeber S, Tsuda M, Wang L, Ozono S, Butleranaka EP, Tanaka YL, Shimizu R, Shimizu K, Yoshimatsu K, Kawabata R, Sakaguchi T, Tokunaga K, Yoshida I, Asakura H, Nagashima M, Kazuma Y, Nomura R, Horisawa Y, Yoshimura K, Takaori-Kondo A, Imai M, Chiba M, Furihata H, Hasebe H, Kitazato K, Kubo H, Misawa N, Morizako N, Noda K, Oide A, Suganami M, Takahashi M, Tsushima K, Yokoyama M, Yuan Y, Genotype to Phenotype Japan (G2P-Japan) Consortium. 2022. Enhanced fusogenicity and pathogenicity of SARS-CoV-2 Delta P681R mutation. *Nature* 602:300–306. <https://doi.org/10.1038/s41586-021-04266-9>.
28. Peacock TP, Sheppard CM, Brown JC, Goonawardane N, Zhou J, Whiteley M, de Silva TI, Barclay WS. 2021. The SARS-CoV-2 variants associated with infections in India, B.1.617, show enhanced spike cleavage by furin. *bioRxiv* <https://doi.org/10.1101/2021.05.28.446163>.
29. Rajah MM, Hubert M, Bishop E, Saunders N, Robinot R, Grzelak L, Planas D, Duflo J, Gellenoncourt S, Bongers A, Zivaljic M, Planchais C, Guivel-Benhassine F, Porrot F, Mouquet H, Chakrabarti LA, Buchrieser J, Schwartz O. 2021. SARS-CoV-2 Alpha, Beta, and Delta variants display enhanced spike-mediated syncytia formation. *EMBO J* 40:e108944. <https://doi.org/10.15252/embj.2021108944>.
30. Hill V, Du Plessis L, Peacock TP, Aggarwal D, Colquhoun R, Carabelli AM, Ellaby N, Gallagher E, Groves N, Jackson B, McCrone JT, O'Toole Á, Price A, Sanderson T, Scher E, Southgate J, Volz E, Barclay WS, Barrett JC, Chand M, Connor T, Goodfellow I, Gupta RK, Harrison EM, Loman N, Myers R, Robertson DL, Pybus OG, Rambaut A. 2022. The origins and molecular evolution of SARS-CoV-2 lineage B.1.1.7 in the UK. *bioRxiv* <https://doi.org/10.1101/2022.03.08.481609>.
31. Liu Y, Liu J, Johnson BA, Xia H, Ku Z, Schindewolf C, Widen SG, An Z, Weaver SC, Menachery VD, Xie X, Shi P-Y. 2022. Delta spike P681R mutation enhances SARS-CoV-2 fitness over Alpha variant. *Cell Rep* 39:110829. <https://doi.org/10.1016/j.celrep.2022.110829>.
32. Kuzmina A, Atari N, Ottolenghi A, Korovin D, Lass IC, Rosental B, Rosenberg E, Mandelboim M, Taube R. 2022. P681 mutations within the polybasic motif of spike dictate fusogenicity and syncytia formation of SARS CoV-2 variants. *bioRxiv* <https://doi.org/10.1101/2022.04.26.489630>.
33. Wilkinson E, Giovanetti M, Tegally H, San JE, Lessells R, Cuadros D, Martin DP, Rasmussen DA, Zekri A-RN, Sangare AK, Ouedraogo A-S, Sesay AK, Priscilla A, Kemi A-S, Oluabusuyi AM, Oluwapelumi AOO, Hammami A, Amuri AA, Sayed A, Ouma AEO, Elargoubi A, Ajayi NA, Victoria AF, Kazeem A, George A, Trotter AJ, Yahaya AA, Keita AK, Diallo A, Kone A, Souissi A, Chtourou A, Gutierrez AV, Page AJ, Vinze A, Iranzadeh A, Lambisia A, Ismail A, Rosemary A, Sylverken A, Femi A, Ibrahim A, Marycelin B, Oderinde BS, Bolajoko B, Dhaala B, Herring BL, Njanpop-Lafourcade B-M, Kleinhans B, McInnis B, et al. 2021. A year of genomic surveillance reveals how the SARS-CoV-2 pandemic unfolded in Africa. *Science* 374:423–431. <https://doi.org/10.1126/science.abj4336>.
34. Sturman LS, Ricard CS, Holmes KV. 1985. Proteolytic cleavage of the E2 glycoprotein of murine coronavirus: activation of cell-fusing activity of virions by trypsin and separation of two different 90K cleavage fragments. *J Virol* 56:904–911. <https://doi.org/10.1128/JVI.56.3.904-911.1985>.
35. Willett BJ, Grove J, MacLean OA, Wilkie C, Logan N, Lorenzo GD, Furnon W, Scott S, Manali M, Szemiel A, Ashraf S, Vink E, Harvey WT, Davis C, Orton R, Hughes J, Holland P, Silva V, Pascall D, Puxty K, da Silva Filipe A, Yebra G, Shaaban S, Holden MTG, Pinto RM, Gunson R, Templeton K, Murcia PR, Patel AH, Haughney J, Robertson DL, Palmarini M, Ray S, Thomson EC. 2022. The hyper-transmissible SARS-CoV-2 Omicron variant exhibits significant antigenic change, vaccine escape and a switch in cell entry mechanism. *medRxiv* <https://doi.org/10.1101/2022.01.03.21268111>.
36. Jaimes JA, Millet JK, Goldstein ME, Whittaker GR, Straus MR. 2019. A fluorogenic peptide cleavage assay to screen for proteolytic activity: applications for coronavirus spike protein activation. *J Vis Exp* 143:e58892. <https://doi.org/10.3791/58892>.
37. Sun X, Tse LV, Ferguson AD, Whittaker GR. 2010. Modifications to the hemagglutinin cleavage site control the virulence of a neurotropic H1N1 influenza virus. *J Virol* 84:8683–8690. <https://doi.org/10.1128/JVI.00797-10>.